GEOFLUIDS

Geofluids (2016) doi: 10.1111/gfl.12191

Quantitative analysis of COH fluids synthesized at HP–HT conditions: an optimized methodology to measure volatiles in experimental capsules

C. TIRABOSCHI[1,2], S. TUMIATI[2], S. RECCHIA[3], F. MIOZZI[2] AND S. POLI[2]

[1]*Dipartimento di Scienze dell'Ambiente e del Territorio e Scienze della Terra, Università degli Studi di Milano Bicocca, Milano, Italy;* [2]*Dipartimento di Scienze della Terra, Università degli Studi di Milano, Milano, Italy;* [3]*Dipartimento di Scienza e Alta Tecnologia, Università degli Studi dell'Insubria, Como, Italy;*

ABSTRACT

The quantitative assessment of COH fluids is crucial in modeling geological processes. The composition of fluids, and in particular their H_2O/CO_2 ratio, can influence the melting temperatures, the location of hydration or carbonation reactions, and the solute transport capability in several rock systems. In the scientific literature, COH fluids speciation has been generally assumed on the basis of thermodynamic calculations using equations of state of simple H_2O–nonpolar gas systems (e.g., H_2O–CO_2–CH_4). Only few authors dealt with the experimental determination of high-pressure COH fluid species at different conditions, using diverse experimental and analytical approaches (e.g., piston cylinder + capsule piercing + gas chromatography/mass spectrometry; cold seal + silica glass capsules + Raman). In this contribution, we present a new methodology for the synthesis and the analysis of COH fluids in experimental capsules, which allows the quantitative determination of volatiles in the fluid by means of a capsule-piercing device connected to a quadrupole mass spectrometer. COH fluids are synthesized starting from oxalic acid dihydrate at P = amb and T = 250°C in single capsules heated in a furnace, and at P = 1 GPa and T = 800°C using a piston-cylinder apparatus and the double-capsule technique to control the redox conditions employing the rhenium–rhenium oxide oxygen buffer. A quantitative analysis of H_2O, CO_2, CH_4, CO, H_2, O_2, and N_2 along with associated statistical errors is obtained by linear regression of the m/z data of the sample and of standard gas mixtures of known composition. The estimated uncertainties are typically <1% for H_2O and CO_2, and <5% for CO. Our results suggest that the COH fluid speciation is preserved during and after quench, as the experimental data closely mimic the thermodynamic model both in terms of bulk composition and fluid speciation.

Key words: capsule-piercing QMS technique, COH fluids, HP-HT experiments, mass spectrometry, piston-cylinder

Received 8 April 2016; accepted 28 July 2016

Corresponding author: Carla Tiraboschi, Dipartimento di Scienze dell'Ambiente e del Territorio e Scienze della Terra, Università degli Studi di Milano Bicocca, piazza della Scienza 4, Milano 20126, Italy.
Email: carla.tiraboschi@unimib.it. Tel: +390264482012. Fax: +390264482073.
Present address: Carla Tiraboschi, Università degli Studi di Milano Bicocca, Milano, Italy

Geofluids (2016)

INTRODUCTION

COH fluids play a fundamental role in many geological processes, influencing the location of devolatilization and melting reactions (e.g., Wyllie 1978; Olafsson & Eggler 1983; Taylor & Green 1988; Wallace & Green 1988; Thibault *et al.* 1992; Jakobsson & Holloway 2008; Thomsen & Schmidt 2008; Foley *et al.* 2009; Grassi & Schmidt 2011; Tumiati *et al.* 2013) and dissolution processes in rock systems (e.g., Walther & Orville 1983; Newton & Manning 2000, 2009; Caciagli & Manning 2003; Shmulovich *et al.* 2006). Most of these processes are dependent on the composition of the COH fluid itself, for instance its XCO_2 [$=CO_2/(CO_2+H_2O)$] ratio. In fact, the bulk composition of COH fluids can be expressed using the basis vector {C, O, H}, but in this case, information regarding the fluid speciation is not directly achievable. Therefore, in most cases, the composition of COH fluids is expressed as a combination of components that represent the actual species forming the fluid itself. The basis vector {H_2O, CO_2, CH_4, CO, H_2, O_2} has been used since many decades to generate the compositional vector space

of COH fluids in thermodynamic calculations (e.g., Connolly & Cesare 1993; Connolly 1995; Huizenga 2001, 2011; Zhang & Duan 2009). However, other neutral (e.g., C_2H_6 and C_3H_8) or charged species (e.g., CO_3^{2-}, HCO_3^-, and CH_3COO^-) (Mysen & Yamashita 2010; Pan *et al.* 2013; Facq *et al.* 2014; Sverjensky *et al.* 2014) have been recently reported in high-pressure COH fluids on the basis of experimental measurements and thermodynamic calculations.

Although several techniques are established for the quantitative analysis of fluids in natural inclusions (e.g., Roedder 1965; Pasteris 1987; Frezzotti *et al.* 1994, 2011; Lamadrid *et al.* 2014), only few works dealt with the analytical determination of the volatile phases in experimental capsules (e.g., Eggler *et al.* 1979; Holloway & Jakobsson 1986; Jakobsson & Holloway 1986; Taylor & Foley 1989; Morgan *et al.* 1992; Jakobsson & Oskarsson 1994; Rosenbaum & Slagel 1995; Matveev *et al.* 1997; Truckenbrodt *et al.* 1997; Truckenbrodt & Johannes 1999; Akaishi *et al.* 2000; Chepurov *et al.* 2012; Dvir *et al.* 2013). In most cases, the speciation of COH fluids in experiments has been estimated on the basis of thermodynamic models that rely on equations of state of simple H_2O–nonpolar gas systems (e.g., equations of state of Connolly & Cesare 1993 and Zhang & Duan 2009). These models have been largely employed to constrain the composition of COH fluids in equilibrium with solid phases, and these latter being routinely analyzed by means of electron microprobe (e.g., Poli *et al.* 2009; Malaspina *et al.* 2010; Goncharov *et al.* 2012; Malaspina & Tumiati 2012; Tumiati *et al.* 2013; Stagno *et al.* 2015). Recently, pioneering more complex models including dissolved species have been developed (Pan *et al.* 2013; Facq *et al.* 2014; Sverjensky *et al.* 2014; Galvez *et al.* 2015), to account for the interaction between fluid and coexisting solid phases, but these models still rely on a very limited experimental dataset.

In this study, we: (i) present a piercing device which allowed to extract quenched COH fluids synthesized in experimental capsules at both ambient and high-pressure conditions; (ii) provide for the first time quantitative analysis of H_2O, CO_2, CH_4, CO, H_2, and O_2 along with analytical uncertainties using quadrupole mass spectrometry; and (iii) compare our experimental result with previous experimental data and thermodynamic models performed in the pure COH system.

Experimental background

Ex situ versus *in situ* experiments in COH-bearing systems

Several analytical techniques have been previously proposed to analyze synthetic high-pressure COH fluids either *in situ* or *ex situ*. *In situ* analyses of COH fluids are generally carried out in hydrothermal diamond anvil cells (HDAC; Bassett *et al.* 1993) coupled with Raman or FTIR spectroscopy (e.g., Sanchez-Valle *et al.* 2003; Mysen & Yamashita 2010; Facq *et al.* 2014; McCubbin *et al.* 2014; Schmidt 2014). These experiments are to date limited to relatively low temperatures and simple chemical systems.

Ex situ analyses are performed on COH fluids equilibrated in experimental capsules and quenched at room temperature and pressure. This method has some advantages compared to *in situ* experiments. First, it is possible to synthesize fluids in a wide range of *P*–*T*–*X* conditions, employing inert noble metal capsules and devices used extensively in experimental petrology for determining phase equilibria (e.g., cold-seal externally heated pressure vessels; piston-cylinder and multi-anvil apparatuses). Second, it is possible to constrain the redox state of the experiment, for instance, using the double-capsule technique (e.g., Eugster & Skippen 1967). Third, fluids can be extracted from the capsule where they have been synthesized and can be analyzed by mass spectrometry, a method that provides great sensitivities for COH species. On the other hand, it is of primary importance to maintain the COH fluid composition during and after the quench process, when the fluid is released from the capsule. Quench and postquench modifications were addressed by some authors (Taylor & Foley 1989; Jakobsson & Oskarsson 1990; Morgan *et al.* 1992; Matveev *et al.* 1997), suggesting that for rapid quench rates (>20°C min^{-1}), the speciation of fluids synthesized at HP–HT conditions is preserved. In any case, quench is not expected to modify the bulk composition of the fluid, expressed in terms of {C, O, H} components, as long as the capsule behaves as a closed system.

The first *ex situ* analysis of COH fluids synthesized in piston-cylinder experiments was performed by Eggler *et al.* (1979) by means of a modified gas chromatograph, using a thermal conductivity detector and an electronic peak integrator. The authors investigated the solubility of CO_2–CO in different silicate melts at $P = 3$ GPa and $T = 1700$°C. To extract the fluid, the capsule was placed at the bottom of a vacuum valve connected to the gas chromatograph. By rapidly closing the valve, the capsule was punctured and the gases were swept to the chromatographic column for the analysis of CO_2 and CO.

Morgan *et al.* (1992) employed silica glass capsules, to analyze the COH fluid generated by thermal dissociation of oxalic acid dihydrate (OAD) by means of Raman spectroscopy. However, due to the brittleness of the capsule material, the investigated conditions of pressure and temperatures were limited to $P < 0.13$ GPa and $T < 750$°C. Moreover, the authors only measured CO_2, CH_4, CO and H_2 while the amount of H_2O was estimated by mass balance calculation, as water presents a weak Raman activity.

Matveev *et al.* (1997) analyzed redox-buffered, graphite-saturated COH fluids at $P = 2.4$ GPa and $T = 1000$°C employing different starting materials (graphite, silver

oxalate, phthalic acid, water, benzoic acid, stearic acid, and anthracene). The capsule was placed in a helium-flushed piercing device connected to a gas chromatograph. Lines were heated to 150°C to prevent water condensation on the tubes without reaching the chromatographic column. The system was calibrated to analyze H_2O, CO_2, C_2H_6, CH_4, CO, and H_2.

Truckenbrodt *et al.* (1997) and Truckenbrodt & Johannes (1999) investigated the COH volatile speciation produced from different organic compounds ($C_4H_4O_4$, $C_9H_{10}O_2$, and $C_{14}H_{22}O$) at $P = 1$ GPa and $T = 900$°C using a gas chromatograph connected to a heated capsule-puncturing system, which allowed to obtain quantitative analyses of H_2, CO, C_2H_6, CO_2, CH_4, and H_2O.

Chepurov *et al.* (2012) investigated serpentine decomposition at high-pressure conditions ($P = 4.5$ GPa, $T = 300$–1000°C). Their chromatographic analysis comprises CO_2, CO, H_2, H_2O, O_2, CH_4, and other hydrocarbons. Also in this case, the gas line was heated to enable the quantitative analysis of H_2O.

Dvir *et al.* (2013) employ diamond traps (Kushiro & Hirose 1992; Baker & Stolper 1994) to collect COH fluids in rocking multi-anvil experiments at $P = 6$ GPa and $T = 1000$°C. The capsules are frozen at $T = -90$°C in liquid nitrogen and open to expose the diamond trap. Fluids are conducted to an infrared gas analyzer by heating the diamond trap at $T = 900$°C for at least 60 sec in a quartz tube. This technique allows determining the H_2O and CO_2 content, at oxidizing conditions, where H_2O and CO_2 are the only COH species stable. In fact, the presence of CO, CH_4, and H_2 could lead to postquench reactions and eventually to a different volatile composition. Quantitative analyses of H_2O and CO_2 were provided with an accuracy and precision of 2–3% and 3–4%, respectively.

Quadrupole mass-spectrometry analyses of COH fluids

The speciation of COH fluids can also be retrieved through quadrupole mass spectrometry (QMS). This method was considered by Jakobsson & Holloway (1986) and Holloway & Jakobsson (1986), which employed a QMS to measure the solubility of a COH fluid in silicate melts at $P =$ 0.5–2.5 GPa and temperatures from 1000 to 1200°C at iron–wustite (IW) oxygen fugacity conditions. The speciation of the fluid (H_2O, CO_2, CO, CH_4, and H_2) was retrieved by heating the melt samples (quenched to a glass) to 1200°C for 5 min under vacuum conditions. The path from the extracting vessel to the QMS was kept short to minimize gas phase reactions, although the authors could not completely exclude postquench reactions.

Taylor & Foley (1989) proposed a capsule-piercing device composed of a modified Whitey regulating valve connected to a mass spectrometer. The technique allowed the analysis of H_2O, CH_4, C_2H_6, and CO_2 generated from stearic acid ($C_{18}H_{36}O_2$) in equilibrium with graphite at pressures from 0.9 to 3.5 GPa and temperatures from 1000 to 1260°C.

Jakobsson & Oskarsson (1994) modified the vacuum valve proposed by Eggler *et al.* (1979) by connecting it to a QMS. The capsule-piercing device was modified to allow the analysis of H_2O by heating the inlet system to 80°C. The authors retrieved the speciation of a COH fluid at iron–wustite oxygen buffer conditions in equilibrium with graphite at pressures from 0.5 to 1 GPa and temperatures from 900 to 1200°C analyzing H_2, CH_4, H_2O, C_2H_6, CO, and CO_2 through a Faraday cup detector.

Rosenbaum & Slagel (1995) investigated the effect of different packing materials on the speciation of COH fluids in piston-cylinder experiments at 0.8 GPa and 800°C, considering single and double-capsule arrangements. Condensable volatile (CO_2 and H_2O) were frozen in liquid N_2 and measured using a manometer (for CO_2) and a pressure gauge (for H_2O). The noncondensable gases were frozen into a sample tube using He and were analyzed through mass spectrometry.

Akaishi *et al.* (2000) synthesized diamonds from graphite and OAD at $P = 7.7$ GPa and $T = 1600$°C. The COH volatile speciation of the fluid (H_2O and CO_2) was analyzed through QMS by piercing the platinum capsule. However, H_2O could not be determined quantitatively, because the inlet system was not heated, and thus, the removal of the adsorbed water in the vacuum chamber was reported to be particularly difficult.

EXPERIMENTAL METHODS: SYNTHESIS OF COH FLUIDS

In this study, COH fluids were generated starting from oxalic acid dihydrate (OAD; $H_2C_2O_4{\cdot}2H_2O$), a solid compound commonly used in high-pressure COH-bearing experiments (e.g., Holloway *et al.* 1968; Holloway & Reese 1974; Kesson & Holloway 1974; Morgan *et al.* 1992; Rosenbaum & Slagel 1995; Draper & Green 1997; Aranovich & Newton 1999; Litvinosky *et al.* 2000; Cherniak & Watson 2007, 2010; McCubbin *et al.* 2014). Two different experimental strategies were considered: (i) single Au capsule loaded with OAD (Fig. 1A), for the synthesis of unbuffered COH fluids at room pressure and $T = 250$°C; (ii) double capsule consisting in an inner $Au_{60}Pd_{40}$ capsule loaded with OAD + glassy carbon spheres, and an outer Au capsule loaded with the redox buffering assemblage Re + ReO_2 + H_2O (RRO) (Fig. 1B), for the synthesis of buffered COH fluids at $P = 1$ GPa and $T = 800$°C.

Synthesis of unbuffered COH fluids P = amb and T = 250°C

Low P and T syntheses were performed heating single gold capsules (OD = 5 mm), filled with approximately 1.5 mg

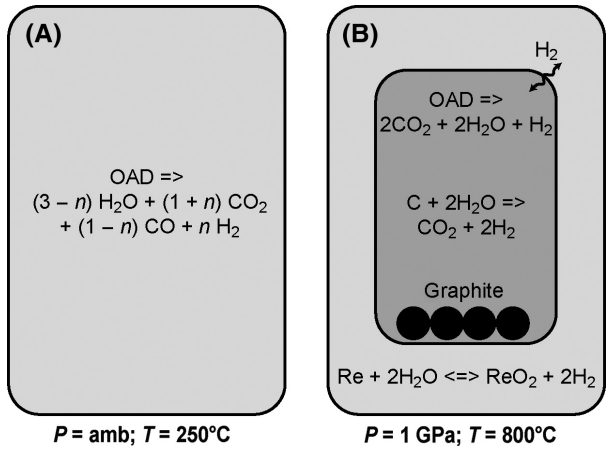

Fig. 1. Capsule arrangements in low-*P*, low-*T* (LP–LT) and high-*P*, high-*T* (HP–HT) experiments. (A) LP–LT: single Au capsule loaded with oxalic acid dihydrate (OAD). Outer diameter 5 mm, wall thickness 0.6 mm. *n* is a parameter, retrieved from direct volatile analysis, that is sensitive to the progress of the water–gas shift reaction (see text); (B) HP–HT: double capsule with the outer Au capsule loaded with rhenium–rhenium oxide and water. Outer diameter 5 mm, wall thickness 0.6 mm. Inner $Au_{60}Pd_{40}$ capsule loaded with OAD and graphite (glassy carbon spheres). Outer diameter 2.3 mm, wall thickness 0.3 mm.

of OAD and seal welded, in a laboratory oven at $T = 250$°C for 2, 5, and 24 h (Fig. 1A). At low temperatures ($T = 230$–350°C), the thermal dissociation of OAD produces H_2O, CO_2, and CO via the reaction:

$$H_2C_2O_4 \cdot 2H_2O \Rightarrow 3H_2O + 1CO_2 + 1CO \quad (R1)$$

Because the capsule behaves as a closed system, the expected composition of the resulting evolved COH fluid should be identical to OAD in terms of {C, O, H} components, while evolved gas species should be H_2O, CO_2, and CO according to reaction R1 (Pernert 1952). However, problems of OAD storage, dehydration, and H_2O absorption could result in fluids that shift to different composition compared to stoichiometric OAD (Boettcher *et al.* 1973; Holloway & Reese 1974; Rosenbaum & Slagel 1995; Truckenbrodt & Johannes 1999; McCubbin *et al.* 2014).

Synthesis of redox-buffered, graphite-saturated COH fluids at *P* = 1 GPa and *T* = 800°C

In carbon-saturated COH system, the composition of the fluid can be constrained through the use of oxygen buffers, which allow calculating the fluid composition through thermodynamic modeling (see Section Thermodynamic modeling of RRO-buffered, graphite-saturated COH fluids). Redox-buffered fluids present therefore a composition constrained by the fO_2 conditions of the system (Eugster & Skippen 1967; Connolly & Cesare 1993), which is different compared to the composition generated by thermal decomposition of OAD. To constrain the redox condition of the graphite-saturated COH fluid, we employ the double-capsule technique (Eugster & Skippen 1967) and the oxygen buffer rhenium–rhenium oxide. The choice of this buffer has been made because of the very low H_2O content in the COH fluid volatile composition predicted by thermodynamic modeling at the investigated conditions, which represents a challenging test for the analytical sensitivity of the proposed procedure.

A seal-welded $Au_{60}Pd_{40}$ inner capsule (OD = 2.3 mm), containing 1.67 mg OAD and 5.5 mg glassy carbon spheres, is placed inside an outer-welded gold capsule (OD = 5 mm) containing the buffering assemblage Re + ReO_2 + H_2O (RRO buffer). As long as Re, ReO_2, and H_2O are present, this buffer fixes the fugacity of O_2 (fO_2^{RRO}) and H_2 (fH_2^{RRO}) through the reactions:

$$Re + O_2 \Longleftrightarrow ReO_2 \quad (R2)$$

and

$$H_2O = H_2 + \frac{1}{2}O_2 \quad (R3)$$

which can be condensed to:

$$Re + 2H_2O \Longleftrightarrow ReO_2 + 2H_2 \quad (R4)$$

In the inner capsule, the dissociation of OAD will produce initially H_2O, CO_2, and H_2 according to the reaction:

$$H_2C_2O_4 \cdot 2H_2O = 2H_2O + 2CO_2 + H_2 \quad (R5)$$

which is different compared to reaction R1 because the water–gas shift reaction:

$$H_2O + CO \Rightarrow CO_2 + H_2 \quad (R6)$$

becomes kinetically favored at high temperature (Holloway *et al.* 1968; Morgan *et al.* 1992).

As the $Au_{60}Pd_{40}$ alloy of the inner capsule is permeable to hydrogen, the fugacity of H_2 is expected to be the same as fH_2^{RRO} in the outer capsule. Indirectly, also all the other species in the COH fluid, including O_2, will be fixed by the RRO buffer. However, as the inner capsule contains a mixed COH fluid and not pure water, the oxygen fugacity in the inner capsule will be lower compared to fO_2^{RRO} (Luth 1989; $fO_2^{RRO} - fO_2^{COH} = -2.48$ log units estimated by thermodynamic calculations, see below). After the quench, the high-pressure COH fluid will exsolve into two fluid phases: (i) a liquid phase consisting mainly of H_2O and (ii) a gaseous phase consisting of noncondensable volatiles (mainly CO_2 at the conditions investigated, see Section Thermodynamic modeling of RRO-buffered, graphite-saturated COH fluids).

Two syntheses characterized by runtimes of 24 and 92 h were carried out at 1 GPa and 800°C in a rocking piston-cylinder apparatus, which allows forward and backward rotations of 180° during the run, thus inverting the position of the loaded capsule in the gravity field. Chemical inhomogeneity within the capsule is in fact common in fluid-bearing experiments (Stalder & Ulmer 2001; Melekhova *et al.* 2007). The rocking piston-cylinder overcomes this problem (Schmidt & Ulmer 2004) as the rotation of the sample induces Rayleigh–Taylor instabilities, forcing the fluid to migrate and favoring chemical re-homogenization. Pressure calibration of the rocking apparatus is based on the quartz to coesite transition (Bose & Ganguly 1995) at $P = 3.12$ GPa and $T = 1000$°C. Capsules were embedded in MgO rods. A corundum disk was placed at the top of the capsule to avoid the direct contact with the thermocouple. The furnace consisted in a graphite heater, surrounded by Pyrex and salt. At the top of the assembly, a pyrophyllite plug was placed to ensure electrical contact. Samples were first pressurized to $P = 0.25$ GPa, heated to $T = 400$°C, and then pressurized and heated simultaneously to the final experimental P–T value. Temperature rate was 50°C min^{-1} until 400 and 100°C min^{-1} to the final value. Temperature was measured with K-type thermocouple and is considered accurate to ±5°C. Experiments were quenched by turning off the power supply with a quench rate of approximately 40°C sec^{-1}. After quenching, the capsules were recovered and cleaned in HCl. The outer capsule was peeled off, and the inner capsule was left in a vacuum oven at 110°C for 2 h to remove any residual water trapped in the RRO buffer stuck on the capsule wall. After the QMS analysis, the pierced capsule is embedded in epoxy and polished, and the persistence of the buffering assemblage RRO is verified by means of scanning electron microscopy (Fig. 2).

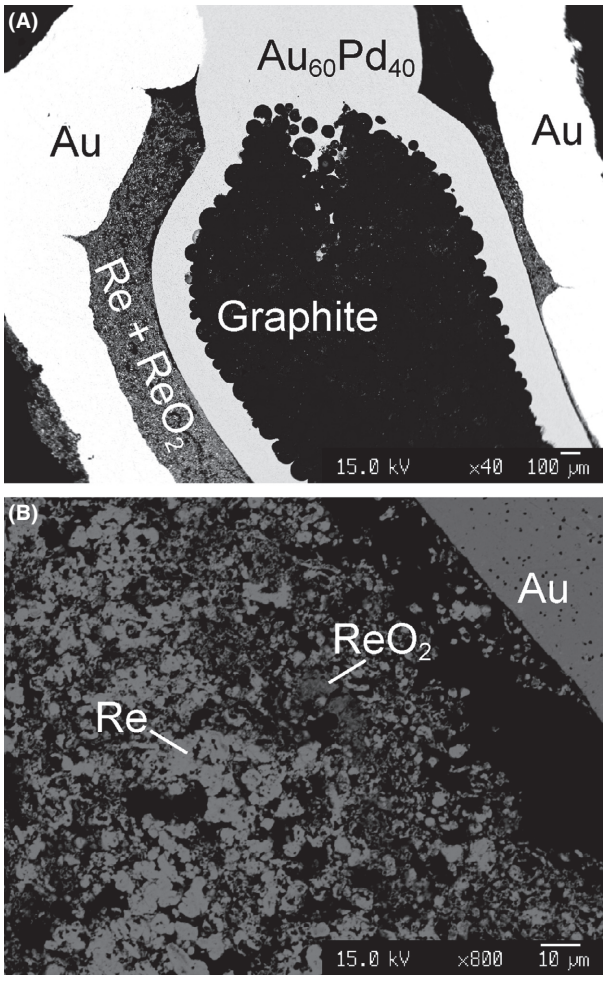

Fig. 2. Backscattered electron (BSE) image of experimental run COH48. (A) Overview of the double capsule; (B) detail of the rhenium–rhenium oxide buffer.

Thermodynamic modeling of RRO-buffered, graphite-saturated COH fluids

The speciation of the graphite-saturated COH fluid in the inner capsule at fH_2^{RRO} conditions was first calculated through thermodynamic modeling (Table 1) using the software package Perplex (Connolly 1990; http://www.perplex.ethz.ch/) and the worksheet Gfluid (Zhang & Duan 2010; http://gcmodel.kl-edi.ac.cn/archives/programs.htm). From a thermodynamic point of view, the speciation of a graphite-saturated fluid is constrained once P, T, and fO_2 are fixed (other details as Supplementary Material). We considered the experimental values of fO_2^{RRO} at $P = 1$ GPa and $T = 800$°C given in Pownceby & O'Neill (1994). The Perplex routine 'fluids' were used to retrieve first fH_2^{RRO} fixed in the outer capsule by RRO buffer (Perplex fluid equation of state no. 16; HSMRK/MRK hybrid; Kerrick & Jacobs 1981; Connolly & Cesare 1993). As the fH_2 of the COH fluid in the inner capsule is equal to fH_2^{RRO}, we calculated the speciation of the COH fluid at 1 GPa, 800°C, and fH_2^{RRO} using a MRK equation of state of graphite-saturated COH fluids (Perplex equation of state no. 11; Connolly & Cesare 1993), retrieving also the fO_2 expected in the inner capsule (Table 1). At these conditions, predicted fluids are mainly composed of CO_2 (92.3 mol%) and H_2O (6.9 mol%), with minor CO, H_2, and CH_4. The volatile composition was also calculated for the same fO_2 conditions, employing the worksheet Gfluid (Zhang & Duan 2010), which provided a similar CO_2-rich composition of the COH fluid, slightly enriched in H_2O (12.9 mol%) (Table 1).

In the double-capsule setting, the composition of the COH fluid becomes enriched in CO_2 compared to the initial fluid composition given by thermal dissociation of OAD. The increase of CO_2 in the fluid is accomplished by R3 and:

Table 1 Volatile speciation of a graphite-saturated COH fluid buffered at rhenium–rhenium oxide hydrogen fugacity conditions (fH_2^{RRO}), calculated assuming μO_2^{RRO} after Pownceby & O'Neill (1994) and thermodynamic modeling (CC93: EoS from Connolly & Cesare 1993; ZD09: EoS from Zhang & Duan 2009). fO_2 out: oxygen fugacity conditions in the outer capsule, where a H_2O-only fluid is present; fH_2 out=in: hydrogen fugacity conditions, fixed at the same value in the inner and in the outer capsule; fO_2 in: oxygen fugacity conditions in the inner capsule, where a COH fluid is present.

P	1 GPa	
T	800°C	
fO_2 out	−11.71	
fH_2 out=in	8.40	
fO_2 in	−14.19	
Thermodynamic model (mol%)		
	CC93	ZD09
H_2O	6.886	12.88
CO_2	92.31	86.35
CH_4	0.002	0.010
CO	0.792	0.730
H_2	0.013	0.003
O_2	0	0

$$C + O_2 = CO_2 \quad (R7)$$

which can be condensed into this water- (and graphite-) consuming reaction:

$$C + 2H_2O = CO_2 + 2H_2 \quad (R8)$$

Water dissociation, H_2 migration in the outer capsule, and graphite oxidation continue until the fH_2 in the inner capsule equals fH_2^{RRO} in the outer capsule.

ANALYTICAL METHODS: THE CAPSULE-PIERCING QMS TECHNIQUE

The volatile content of the synthesized COH fluids has been measured using a capsule-piercing device (Fig. 3) connected to a quadrupole mass spectrometer (QMS). A schematic overview of the capsule-piercing device is provided in Fig. 3E. The device consists of three parts: (i) a Teflon–steel extraction vessel (reactor), inspired by that proposed by Manning & Boettcher (1994) (Fig. 3B); (ii) an electric furnace, where the vessel is heated (Fig. 3A), and (iii) a heated gas manifold system, connected to the QMS, the standard and carrier gas tanks, and the vacuum pump.

The reactor is composed of a base part (Fig. 3D), where the capsule is placed, and a top part (Fig. 3C), where a steel mill is mounted. Both the base and the top of the reactor are threaded so that the base can be driven upward with a screwing action. The external part of the base is mantled by a steel liner to reduce volume variations due to the high thermal expansion of Teflon (Fig. 3B). Openings on the top allow the inert gas carrier (ultrapure Ar) to flow inside the reactor. The presence of an O-ring ensures a tight seal. The capsule, placed horizontally and partially embedded in epoxy, is allocated on a cross steel support, designed to oppose the rotation given by the steel pointer during the piercing (Fig. 3D). To puncture the capsule, the base is screwed upward with a hex key until the steel mill pierces the capsule. Before the piercing occurs, the reactor needs to be evacuated from all the residual contaminants (e.g., air and condensed water) using a vacuum pump. Then, the reactor is conditioned with Ar through a five-way valve (V1 in Fig. 3E), useful to select also the calibrating gas mixtures, employed as standards for the QMS analysis. The flow rate is selected through a mass flow controller (El-Flow Bronkhorst® High-Tech). Lines are heated to 80°C in order to avoid water condensation. Also the reactor, enclosed in a furnace (Fig. 3B), is heated at 80°C, so that all volatiles released from the capsule after the piercing, including H_2O, can be transported to the QMS by the gas carrier.

The pressure conditions of both the line and the reactor are monitored through high-resolution sensor gauges (±1 mbar error). The temperatures of the line, reactor, and furnace are monitored with K-type thermocouples, controlled through a Eurotherm nanodac™ PID data controller and recorder. The quadrupole mass spectrometer is an EXXTORR 0–200 amu, Mod. XT 200. It is equipped with two detectors: (i) a Faraday cup and (ii) a secondary electron multiplier (SEM), which is more sensitive to low concentrations of gases compared to the Faraday cup. Due to the very small amount of volatiles contained in the experimental capsule, analyses have been always performed with SEM. For every *m/z* channel, 310 points are registered, one point every 5 sec, for a total time of 1550 sec.

Determination of the reactor volume

We retrieved the amount of gases evolved from the capsule after the piercing using the ideal gas law:

$$n = \Delta P * V_r/(R * T), \quad (R9)$$

where n are the moles of the evolved gases, ΔP [mbar] is the pressure increase in the reactor after the piercing, V_r [L] is the volume of the reactor, R is the universal gas constant [83.145 L mbar K^{-1} mol^{-1}], and T [K] is the temperature of the reactor when the capsule is pierced. While ΔP and T are monitored, the volume of the reactor needs to be constrained. The reactor chamber volume is variable as it depends on the number of rounds performed when the base part is screwed to the top. Consequently, the reactor chamber volume V_r is a function of the distance between the base and the top part (h in Fig. 3E). V_r was retrieved for three different values of h: 6, 8, and 10 mm.

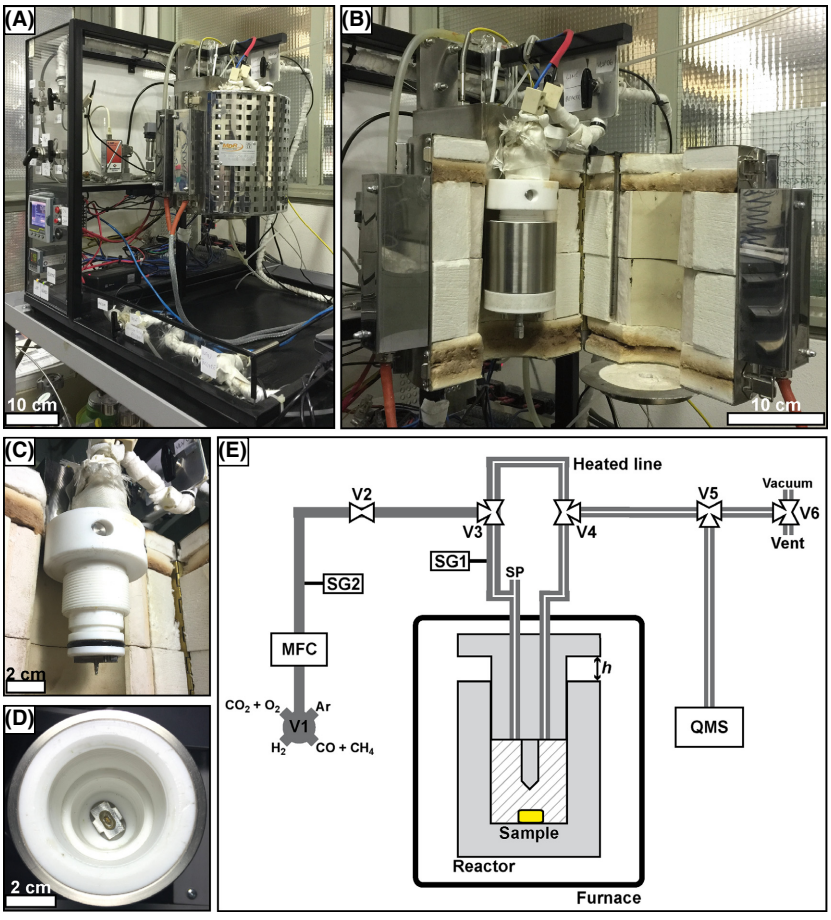

Fig. 3. The capsule-piercing device. (A) Overview of the device and the control panel; (B) the Teflon/steel reactor placed in the furnace; (C) top part of the reactor; (D) lower part of the reactor with the capsule mounted in epoxy, placed on the cross steel support; (E) schematic drawing of the capsule-piercing QMS device. MFC, Mass Flow Controller; SG1, high-resolution sensor gauge to measure the reactor pressure; SG2, high-resolution sensor gauge to measure the line pressure; V1, five-way valve used to select standard gas mixtures or the gas carrier; V3 and V4, valves to insulate the reactor during the piercing; V5, valve to convoy the gas to the QMS; SP, silicon septum employed for H2O calibration; *h*, know distance between the top and the base of the reactor; QMS, quadrupole mass spectrometer. Both the reactor and the lines connecting the reactor to the QMS are heated at 80°C.

The volume of the reactor for a fixed h is determined by filling it with a constant flux of Ar (Φ = 3 Nml min^{-1}) until the pressure reaches 500 mbar. The volume is retrieved through the equation:

$$V_r = [(\Phi/273.15) * T * t_r)]/\Delta P, \quad \text{(R10)}$$

where t_r is the time employed to reach the value of 500 bar, Φ [L/s] is the flux of Ar that is corrected for the calibration temperature of the mass flow controller (MFC) (273.15 K), and T is the temperature of the reactor, expressed in [K].

Volumes at h = 6, 8, and 10 mm were fitted through linear regression analysis (LRA) (Fig. 4). The coefficients retrieved from LRA (α = *y*-intercept and β = slope) were substituted to express the volume of the reactor depending on the h value:

$$V_r = h * \beta + \alpha \quad \text{(R11)}$$

By substituting Eq. R11 in R9, the number of moles released from the capsule is derived using the following equation:

$$n = \Delta P * (h * \beta + \alpha)/(R * T) \quad \text{(R12)}$$

Calibration of the QMS analysis

During the QMS analysis, mass/charge (m/z) channels are monitored to measure the volatile species H_2O, CO_2, CH_4, CO, H_2, O_2, and air/N_2 (Table 2). Due to chemical fragmentation, a species can contribute on more than one channel. For instance, CO_2 is fragmented to C^+ and CO^+, so it contributes to channels 12 and 28 in addition to 44. Moreover, as CO and CH_4 fragment C^+ as well, the mass/charge channel relative to carbon (m/z = 12) will also register the contributes from the two carbon-bearing species. To perform quantitative analyses of COH fluids, we employed as standards double-distilled water and three gas mixtures with known composition: (i) Ar + CO_2 (10 vol.%) + O_2 (9.85 vol.%); (ii) Ar + H_2 (10 vol.%); and (iii) Ar + CH_4 (10 vol.%) + CO (10 vol.%). For each standard, the contribution of the species on the m/z channels, derived by integration of the QMS signal over time and normalized to 1 micromole, is gathered into a calibration matrix (Table S1).

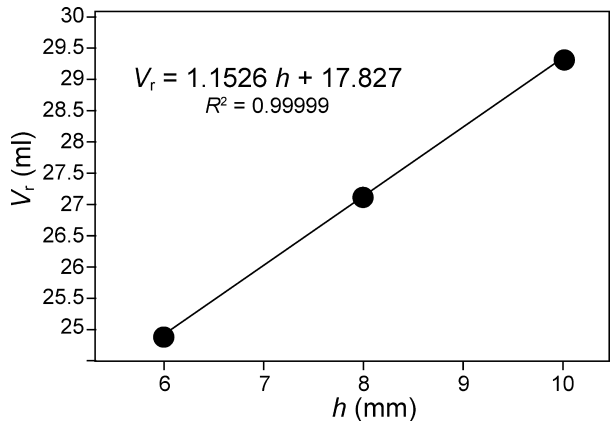

Fig. 4. Calibration curve of the reactor chamber volume (V_r) plotted as a function of h (see Fig. 3).

Table 2 Mass/charge (m/z) channels monitored during QMS analysis and relative contribution of the chemical species of interest.

m/z	H_2O	CO_2	CH_4	CO	H_2	O_2	N_2	Ar
2	X		X		X			
12		X	X	X				
14			X				X	
15			X					
18	X							
20								X
28		X		X			X	
32						X		
44		X						

Water calibration is achieved by charging in the reactor a known amount of water (1 µl) with a Hamilton microsyringe (head space type) through a silicon septum placed at the top of the reactor (SP in Fig. 3E). Calibration with gas mixtures is performed by filling the reactor until the pressure in the reactor reaches a defined value of 500 mbar. The number of gas moles is then determined through Eq. R12.

The QMS analysis provides also the amount of atmospheric air (and/or N_2) present either in the reactor or in the capsule. In this case, air is used as standard. The m/z channels monitored are 14 and 28 for N_2 and 32 for O_2.

Capsule-piercing QMS analysis of COH fluids

After the run has been completed, the experimental capsules are mounted on a cross steel support placed at the bottom of the reactor. The reactor is then screwed upward to a certain height (h in Fig. 3E), to retrieve the reactor chamber volume from Eq. R11. The furnace is closed and heated to $T = 80$°C. The line and reactor preconditioning are accomplished by performing pressurization/venting cycles with Ar. Before the piercing occurs, the reactor is bypassed from the line (V3 and V4 in bypass position). This allows monitoring the pressure variation (ΔP) inside the reactor once that the gases are released during the piercing. By rotating the hex key connected to the reactor, the base part of the reactor moves upward toward the steel mill. As the volume decreases, the pressure registered by the sensor gauges increases. Once that the steel mill pierces the capsule, a sudden increase in the reactor pressure reveals the release of the capsule volatiles in the reactor chamber. Then, the reactor is screwed downward to the initial h value.

The pressure (ΔP) generated by the release of COH fluids during the piercing and the reactor temperature are employed to retrieve the total moles of the COH volatile species through Eq. R12.

Before valves V3 and V4 are opened for the QMS analysis, the inner pressure is decreased to zero so that the released gases are conveyed to the QMS at a controlled carrier gas flow (10 Nml min^{-1}).

Once the areas for each m/z channels are obtained, least square regression is employed to transform the m/z data into H_2O, CO_2, CH_4, CO, H_2, O_2, and air/N_2 components expressed as micromoles of volatiles, using the calibration matrix (see Section Calibration of the QMS analysis). In practice, linear regression is used to solve a linear overdetermined system composed of eight equations:

$$A'_i = \sum_{j=1}^{7} n_j * A_{ij}, \tag{R13}$$

where A_{ij} is the m/z signal areas determined by the calibration of each volatile species j, A'_i is the m/z signal area of the sample, and n_j is the unknown number of moles of the j species in the sample (Fig. 5B).

The integration of the QMS m/z signals and the regression is performed using a customized routine developed as a Mathematica® notebook. For every species, the Mathematica® notebook provides the standard error of the model, the t-statistic and the P-value, in addition to the parameter R^2, adjusted R^2, the Akaike's information criterion (AIC), and the Bayesian information criterion (BIC) (Fig. 4C). AIC is useful to evaluate how many information is lost between a proposed model and the real dataset. BIC allows selecting the best model between a set of possible models with different number of parameters. Increasing the number of parameters in a model leads to an increase of the likelihood function but at the same time can leads to an over-fitting of the data. BIC mitigates the risk of over-fitting using a penalization term, which is function of the number of parameters used in the model. Because of the numerical definition of both terms, an increase of the likelihood function leads to a decrease of the AIC and BIC value. A large negative value for the two terms means that the likelihood function is high and real data are well represented by the chosen model.

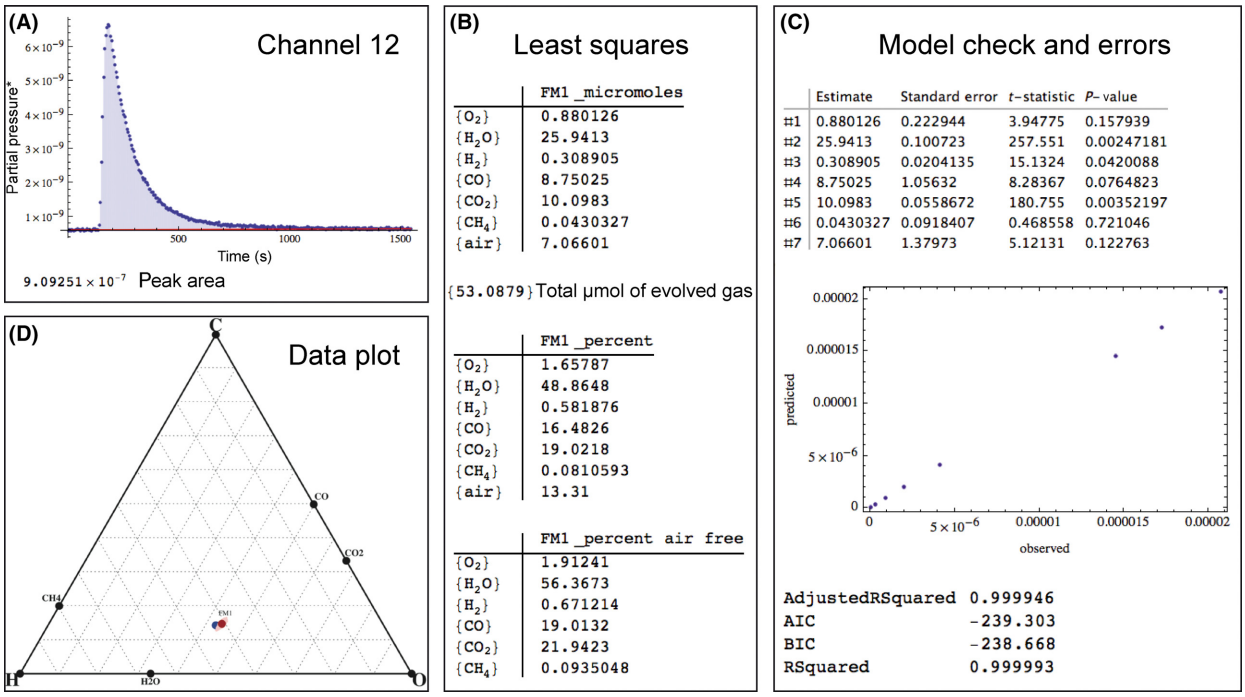

Fig. 5. Output results from data reduction performed through the Mathematica® routine. (A) *m/z* signal integration (peak area). An example for channel 12 is shown here. On the *y*-axis (partial pressures*) values represent partial pressures (torr) multiplied by an unconstrained SEM (Secondary Electron Multiplier) enhancing factor; (B) least square model, performed using the calibration matrix and the integrated *m/z* signals of the sample. Data are given in micromoles, mol%, and mol% on a air-free basis; (C) model check and errors. In this section are given the number of moles estimated by the least square model and the associated standard error, *t*-statistic, and *P*-value. On the *x*-axis, the experimental results are plotted against the calculated model. The parameter R^2, adjusted R^2, the Akaike's information criterion and the Bayesian information criterion are also provided; (D) sample data plot on the COH ternary diagram (red dot). The analytical uncertainty, simulated by means of Monte Carlo on the basis of the standard error of the least square model (light red), and the reference point (stoichiometric oxalic acid dihydrate; blue dot) are also shown in the COH diagram.

The bulk composition of the COH fluid is then plotted on a ternary C–O–H diagram (Fig. 5D) and can be compared with the starting composition of OAD and, when possible, the thermodynamic model of the fluid. The propagation of the standard errors for each volatile species, corresponding to the analytical uncertainty, is calculated through Monte Carlo simulations, and it is shown in the C–O–H diagram as a cloud of uncertainty. At the investigated concentrations, the relative standard errors are typically <1% for H_2O, CO_2, CH_4, H_2, and O_2, and <5% for CO.

RESULTS

Synthesis of unbuffered COH fluids at *P* = amb and *T* = 250°C

Four syntheses were performed at $T = 250$°C, ambient pressure, and run times of 2, 5, and 24 h, to analyze the volatile species generated by thermal decomposition of OAD. Experimental results are provided in Table 3.

Gas evolved from experiment FM1 (2 h) generates a ΔP of 48 mbar corresponding to 41.13 µmol of volatiles. The retrieved volatile phase composition consists mainly of H_2O (56.37 ± 0.22 mol%), CO_2 (21.94 ± 0.12 mol%), and CO (19.01 ± 2.30 mol%) (Table 3). Minor quantities of O_2 (1.91 ± 0.48 mol%), H_2 (0.67 ± 0.04 mol%), and CH_4 (0.09 ± 0.20 mol%) were also detected.

Experiment COH41 (2 h) is characterized by $\Delta P = 57$ mbar corresponding to 48.84 µmol of volatiles. Compared to experiment FM1, similar water contents were detected (57.11 ± 0.38 mol%) accompanied by higher content of CO_2 (32.78 ± 0.21 mol%) and lower CO (7.26 ± 4.08 mol%) (Table 3). H_2 (2.79 ± 0.08 mol%) and CH_4 (0.07 ± 0.35 mol%) were also identified.

Experiment COH73 was performed for a run time of 5 h. The piercing generates a ΔP of 38 mbar from the release of 31.84 µmol of H_2O (53.92 ± 0.58 mol%), CO_2 (33.51 ± 0.32 mol%), CO (8.96 ± 6.12 mol%), and minor H_2 quantities (3.51 ± 0.12 mol%) (Table 3).

Gas evolved from the piercing of experiment COH74 (runtime = 24 h) provides a ΔP of 40 mbar corresponding to 34.05 µmol of volatiles. Compared to experiment COH73, the COH fluid presents extremely similar amounts of H_2O (53.23 ± 0.60 mol%), CO_2 (32.65 ± 0.33 mol%), CO (10.01 ± 6.26 mol%), and H_2 (3.27 ± 0.21 mol%) (Table 3).

Table 3 Volatile speciation of the LP–LT syntheses and HP–HT syntheses of graphite-saturated COH fluids buffered at fH_2^{RRO} measured by quadrupole mass spectrometry. The total amount of fluid evolved from the capsule is expressed in μmol and is retrieved from the ideal gas law $PV = nRT$. The amount of the monitored species (μmol) derived from linear regression analysis performed through Mathematica notebook. Negative values should be considered zero values as correspond to fictitious values given by the least-squares model. The volatile speciation of the COH fluid is expressed as moles percentage on an air- and N_2-free basis (mol%*).

	FM1	COH41	COH73	COH74	COH48	COH49
P	amb	amb	amb	amb	1 GPa	1 GPa
T	250°C	250°C	250°C	250°C	800°C	800°C
Runtime (h)	2	2	5	24	24	92
μmol tot	41.13	48.84	31.84	34.05	23.75	27.38
μmol						
H_2O	25.94 (0.10)	15.60 (0.11)	5.114 (0.06)	3.466 (0.04)	0.264 (0.03)	0.643 (0.03)
CO_2	10.10 (0.06)	8.953 (0.06)	3.178 (0.03)	2.126 (0.02)	7.887 (0.02)	10.26 (0.02)
CO	8.750 (1.06)	1.981 (1.11)	0.850 (0.58)	0.652 (0.41)	−0.326 (0.32)	0.205 (0.37)
CH_4	0.043 (0.09)	0.018 (0.10)	−0.005 (0.05)	0.014 (0.04)	−0.003 (0.03)	0.006 (0.03)
H_2	0.310 (0.02)	0.762 (0.02)	0.344 (0.01)	0.213 (0.01)	−0.007 (0.01)	−0.018 (0.01)
O_2	0.880 (0.22)	–	−0.005 (0.12)	–	–	0.004 (0.08)
N_2	–	0.316 (1.22)	–	0.040 (0.45)	0.555 (0.35)	–
air	7.066 (1.38)	3.188 (0.55)	1.478 (0.76)	1.091 (0.20)	1.124 (0.16)	2.343 (0.48)
mol%*						
H_2O	56.37 (0.22)	57.11 (0.38)	53.92 (0.58)	53.23 (0.60)	3.233 (0.37)	5.781 (0.31)
CO_2	21.94 (0.12)	32.78 (0.21)	33.51 (0.32)	32.65 (0.33)	96.77 (0.21)	92.28 (0.17)
CO	19.01 (2.30)	7.256 (4.08)	8.956 (6.12)	10.01 (6.26)	0	1.846 (3.29)
CH_4	0.094 (0.20)	0.068 (0.35)	0	0.218 (0.54)	0	0.054 (0.29)
H_2	0.671 (0.04)	2.790 (0.08)	3.506 (0.12)	3.272 (0.12)	0	0
O_2	1.912 (0.48)	0	0	0	0	0.035 (0.69)

Synthesis of redox-buffered, graphite-saturated COH fluids at $P = 1$ GPa and $T = 800$°C

Two syntheses of redox-buffered, graphite-saturated COH fluids, performed at 1 GPa and 800°C employing a rocking piston-cylinder apparatus and the double-capsule technique, were carried out at different run times of 24 h and 92 h. The experimental conditions and results are reported in Table 3.

The fluid released form experiment COH48 (24 h) generated a ΔP of 28 mbar, corresponding to 23.75 μmol of volatiles. The analyzed fluid is CO_2 rich (96.77 ± 0.21 mol%) with minor quantities of H_2O (3.23 ± 0.37 mol%) (Table 3).

Fluid in experiment COH49 (92 h) presents a similar composition compared to the experiment COH48: 92.28 ± 0.17 mol% of CO_2 and 5.78 ± 0.31 mol% of H_2O. Minor quantities of CO (1.84 ± 3.29 mol%), CH_4 (0.05 ± 0.29 mol%), and O_2 (0.04 ± 0.69 mol%) were also detected. In this case, the registered ΔP was 32 mbar corresponding to 27.38 μmol of volatiles.

DISCUSSION

Unbuffered COH fluids at P = amb and $T = 250$°C

In Fig. 6, the compositions of fluids generated by thermal decomposition of OAD at P = amb and $T = 250$°C are plotted in a C–O–H ternary diagram (colored dots) together with their cloud of uncertainty (gray dots) and compared to the stoichiometric composition of OAD (black dots) (Fig. 6A). For all the experiments, fluid compositions in terms of {C, O, H} components plot very close to OAD composition within analytical uncertainty, as expected in single capsules, where no mass transfers with the external environment are expected (Fig. 6B). However, we observed a minor shift of all the experimental results compared to the stoichiometric OAD composition, most probably due to H_2 loss, as reported in Morgan *et al.* (1992). Moreover, the speciation of COH fluids in terms of components {H_2O, CO_2, CH_4, CO, H_2, O_2} shows some differences (Table 3).

Experimental two-hour runs, FM1 and COH41, present nearly identical percentages of H_2O (56.37 mol% and 57.11 mol%, respectively). However, experiment COH41 shows higher quantity of CO_2 (32.78 mol%) compared to FM1 (21.94 mol%). The two experiments with longer run times (5 and 24 h) present similar volatiles composition similar to COH41, for what concerns H_2O (53.92 mol% and 53.23 mol%), CO_2 (33.51 mol% and 32.65 mol%), and H_2 (3.51 mol% and 3.27 mol%). We observe an increase in CO content from 8.96 mol% to 10.01 mol% from the 5- to 24-h experimental run. These differences in the COH fluid speciation suggest the presence of kinetic effects at the investigated low-T conditions and a consequent different progress of the water–gas shift reaction R6. Morgan *et al.* (1992), investigating the dissociation of OAD, proposed the following reaction to account for the formation of different volatiles in the experimental charge:

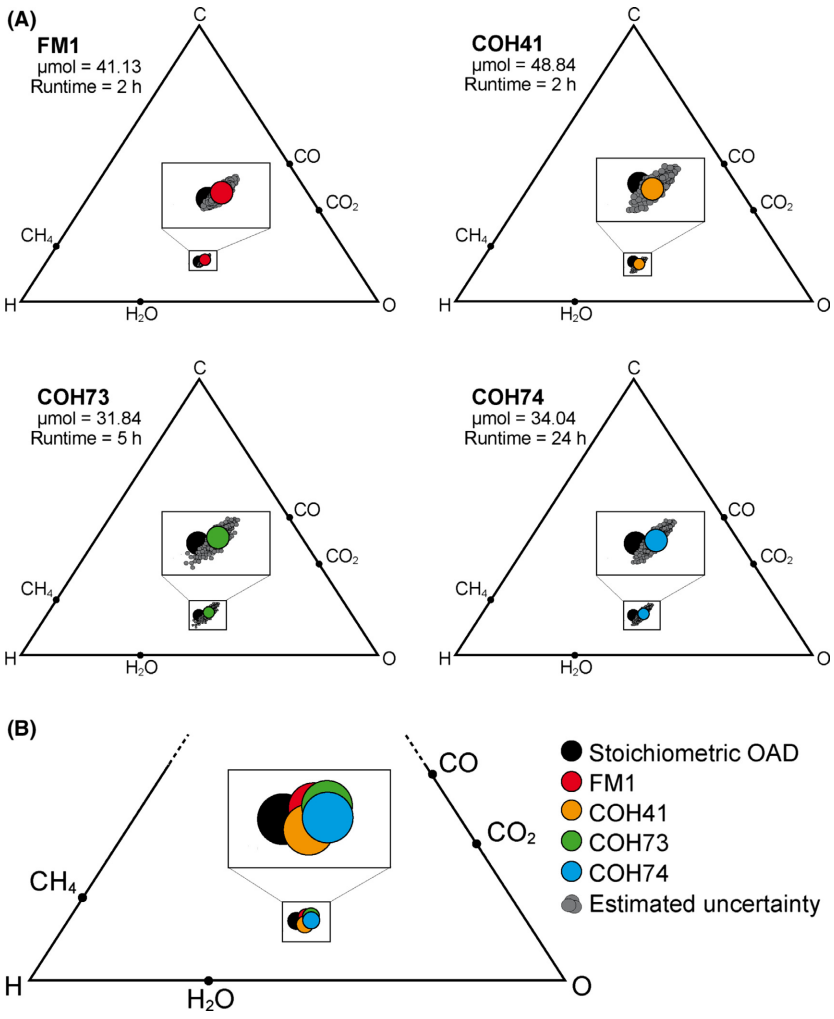

Fig. 6. COH ternary diagram for unbuffered COH fluids synthesized at room pressure and $T = 250°C$. Black dots: stoichiometric oxalic acid dihydrate composition; colored dots: COH fluid composition retrieved by the capsule-piercing QMS technique. (A) Ternary diagrams for experiments performed at 2 h, 5 h, and 24 h. Grey dots: uncertainty cloud retrieved through Monte Carlo simulation. The number of moles of volatile species is also provided. (B) Summary plot of the samples shown in A.

$$H_2C_2O_4 \cdot 2H_2O = (3-n)H_2O + (1+n)CO_2 + (1-n)CO + nH_2 \quad \text{(R14)}$$

where n is a parameter, retrieved from direct volatile analysis, that is sensitive to the progress of the water–gas shift reaction (R6), being zero when R6 does not occur and one when R6 is completed. On the basis of our measurements, at the investigated conditions, the parameter n spans from 0.08 (FM1) to 0.39 (COH41), 0.41 (COH74), and 0.43 (COH73). At $T = 230°C$ (runtime = 1.1 h), Morgan *et al.* (1992) found a n parameter of 0.1, which is comparable to the two-hour experiment FM1, but substantially lower compared to long-duration experiments COH73 and COH74, suggesting that the achievement of equilibrium in these fluids is nonstraightforward for run times <5 h. In addition, it is worth noting that Morgan *et al.* (1992) did not directly measure H_2O, which was estimated through mass balance calculations, which could have introduced high uncertainties in the estimate of the n parameter.

Redox-buffered, graphite-saturated COH fluids at $P = 1$ GPa and $T = 800°C$

Syntheses of a graphite-saturated COH fluid at 1 GPa and 800°C were performed at controlled redox conditions buffered by RRO in double capsules. Therefore, their composition can be compared with model compositions retrieved from thermodynamic calculations performed in the C-O-H system (Table 1) for the same P, T, and fH_2^{RRO} conditions. As reported in Fig. 7A, the COH composition of the two fluids run for 24 h (COH 48) and 92 h (COH 49) plot both on the model graphite saturation surface, suggesting the achievement of equilibrium with graphite (cf. Matveev *et al.* 1997). Compared to the initial bulk composition of OAD (black dots in Fig. 7A), the measured volatile composition of the double-capsule synthesis is shifted toward CO_2, as predicted by thermodynamic models (squares in Fig. 7A). The equilibration of the COH fluid is accomplished through reaction R8, which produces CO_2 and H_2 at the expenses of H_2O and graphite. After 24 h, the

volatile speciation of the COH fluid (Table 3) is comparable to the thermodynamic models (Fig. 7A; Table 1), being only slightly enriched in CO_2 (96.77 mol% CO_2) compared to the thermodynamic model based on the EoS of Connolly & Cesare (1993) (92.3 mol% CO_2; approximately +5 mol %; Fig. 7A). Compared to the thermodynamic model based on the EoS of Zhang & Duan (2009), the experimental results are more CO_2 enriched (86.35 mol% CO_2; approximately +10 mol%; Fig. 7A). However, we must note that the modeled volatile composition is extremely sensitive to small variations in the oxygen fugacity. In fact, the same fluid composition retrieved from the EoS of Connolly & Cesare (1993) (see Table 1) can be obtained by slightly varying the $\log fO_2$ in the Zhang & Duan (2010) model from −14.19 to −14.16.

This minor difference between experimental data and thermodynamic models tends to zero in the 92-h synthesis, where the volatiles speciation is almost identical to the Connolly & Cesare (1993) thermodynamic model (92.28 mol% CO_2; Fig. 7A). However, it is worth to note that the volatile composition of experiment COH49 (92 h) lies within the error given by the volatile composition from experiment COH48 (24 h) (Fig. 7B); consequently, we suggest that equilibrium conditions can be accomplished already with a run time of 24 h.

Our results indicate that the COH fluid speciation is preserved during and after quench, as the experimental data closely mimic the thermodynamic model both in terms of bulk composition and fluid speciation. Moreover, heating the reactor and the transfer line at $T = 80°C$ does not affect the volatile speciation of the COH fluid during the path from the reactor to the QMS.

Differently to other COH fluid syntheses performed with single capsules (Eggler *et al.* 1979; Holloway & Jakobsson 1986; Taylor & Foley 1989; Jakobsson & Oskarsson 1990; Matveev *et al.* 1997), we employed the double-capsule technique, which allows buffering the fluids at controlled redox and fH_2 conditions. The volatile speciation is in fact highly dependent on the H_2-absorbing capacity of the material that surrounds the capsule during the experimental run (Rosenbaum & Slagel 1995). By employing the double-capsule technique, the COH fluid is synthesized in a capsule not in direct contact with the packing material. The outer Au capsule provides a significant amount of H_2O to account for the H_2 loss, and it contains the buffering assemblage Re + ReO_2 + H_2O that fix the hydrogen (and oxygen) fugacity conditions during the run. Our measurement of the volatile speciation of buffered COH fluid confirms that the double-capsule technique is a reliable technique to synthesize compositionally constrained COH fluids (Rosenbaum & Slagel 1995). The capsule-piercing QMS technique has been proved to be a valuable choice even for the analysis of fluids containing low amount of water, which is the most challenging COH species to analyze *ex situ*, mainly due to the difficulties in transporting it to the quadrupole mass spectrometer. We were able to detect extremely low amounts of water (e.g., 0.26 μmol from experiment COH48) with an analytical error <0.6%.

CONCLUSIONS

The capsule-piercing QMS technique allows retrieving *ex situ* the volatile composition and speciation of COH fluids

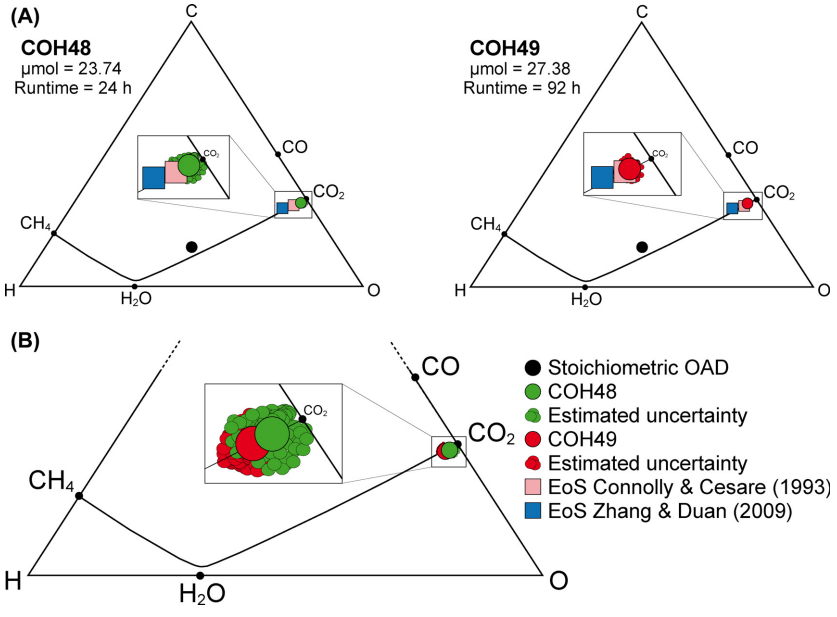

Fig. 7. COH ternary diagram for graphite-saturated COH fluids, buffered at fH_2^{RRO}, synthesized at 1 GPa and 800°C. Black dot: stoichiometric oxalic acid dihydrate composition; colored dots: COH fluid composition retrieved by the capsule-piercing QMS technique. Black solid line: graphite saturation surface (Connolly 1995) calculated by thermodynamic modeling (EoS Connolly & Cesare 1993), representing the boundary between the fluid- and the fluid + graphite fields. (A) Ternary diagrams for experiments performed at 24 h and 92 h. Small colored dots: uncertainty cloud retrieved through Monte Carlo simulation. Colored squares: graphite-saturated COH fluid composition calculated through thermodynamic models. The number of moles of volatile species is also provided. (B) Summary plot of the samples shown in A.

in experimental capsules. Our technique provides quantitative analysis of the main volatile species in the COH system: H_2O, CO_2, CH_4, CO, H_2, and O_2. Moreover, the technique allows measuring air and/or N_2 contained in the capsule or leaking into the line. We provide for the first time a measure of volatiles, in terms of micromoles, obtained using standard gas mixtures. Our approach is an effective way to synthesize and analyze COH fluids at various *P* and *T* conditions, suitable also for volatile contents <1 micromole. Quadrupole mass spectrometry ensures superior performances in terms of selectivity of molecules to be detected, high acquisition rates, and extended linear response range. Heated lines and reactor allow the analysis of H_2O with relatively low uncertainties. The capsule-piercing QMS technique could represent a routine approach for the analyses of volatiles in fluid-saturated experiments. The fluid composition and speciation are in fact preserved after the piercing. The experimental capsule is not destroyed during the piercing operation, so it is possible to prepare the sample for further characterization (e.g., electron microprobe analysis). This would allow to directly measuring the volatile speciation to evaluate whether an experimental strategy provides the same species predicted by thermodynamic calculations or whether dissolved species influence the volatile speciation of the fluid.

ACKNOWLEDGEMENTS

This research was supported by the Italian Ministry of Education, University and Research (MIUR) program PRIN2012R33ECR. C.T., S.T., and S.P. acknowledge supports from the Deep Carbon Observatory (DCO). D. Spanu is thanked for the assistance in calibrating the device. Reviews by R.W. Luth and an anonymous referee significantly improved the manuscript. The authors have no conflict of interest to declare.

REFERENCES

Akaishi M, Kumar S, Kanda H, Yamaoka S (2000) Formation process of diamond from supercritical H_2O–CO_2 fluid under high pressure and high temperature conditions. *Diamond and Related Materials*, **9**, 1945–50.

Aranovich LY, Newton RC (1999) Experimental determination of CO2–H2O activity-composition relations at 600–1000°C and 6–14 kbar by reversed decarbonation and dehydration reactions. *American Mineralogist*, **84**, 1319–32.

Baker MB, Stolper EM (1994) Determining the composition of high-pressure mantle melts using diamond aggregates. *Geochimica et Cosmochimica Acta*, **58**, 2811–27.

Bassett WA, Shen AH, Bucknum M, Chou IM (1993) A new diamond anvil cell for hydrothermal studies to 2.5 GPa and from 190 to 1200°C. *Review of Scientific Instruments*, **64**, 2341–5.

Boettcher AL, Mysen BO, Allen JC (1973) Techniques for the control of water fugacity and oxygen fugacity for experimentation in solid-media high-pressure apparatus. *Journal of Geophysical Research*, **78**, 5898–901.

Bose K, Ganguly J (1995) Quartz-coesite transition revisited: reversed experimental determination at 500–1200°C and retrieved thermochemical properties. *American Mineralogist*, **80**, 231–8.

Caciagli NC, Manning CE (2003) The solubility of calcite in water at 6–16 kbar and 500–800°C. *Contributions to Mineralogy and Petrology*, **146**, 275–85.

Chepurov AI, Tomilenko AA, Zhimulev EI, Sonin VM, Chepurov AA, Kovyazin SV, Timina TY, Surkov NV (2012) The conservation of an aqueous fluid in inclusions in minerals and their interstices at high pressures and temperatures during the decomposition of antigorite. *Russian Geology and Geophysics*, **53**, 234–46.

Cherniak DJ, Watson EB (2007) Ti diffusion in zircon. *Chemical Geology*, **160**, 383–90.

Cherniak DJ, Watson EB (2010) Li diffusion in zircon. *Contributions to Mineralogy and Petrology*, **242**, 470–83.

Connolly JAD (1990) Multivariable phase diagrams; an algorithm based on generalized thermodynamics. *American Journal of Science*, **290**, 666–718.

Connolly JAD (1995) Phase diagram methods for graphitic rocks and application to the system C–O–H–FeO–TiO_2–SiO_2. *Contributions to Mineralogy and Petrology*, **119**, 94–116.

Connolly JAD, Cesare B (1993) C–O–H–S fluid composition and oxygen fugacity in graphitic metapelites. *Journal of Metamorphic Geology*, **11**, 379–88.

Draper DS, Green TH (1997) P-T phase relations of silicic, alkaline, aluminous mantle-xenolith glasses under anhydrous and C–O–H fluid-saturated conditions. *Journal of Petrology*, **38**, 1187–224.

Dvir O, Angert A, Kessel R (2013) Determining the composition of C–H–O liquids following high-pressure and high-temperature diamond-trap experiments. *Contributions to Mineralogy and Petrology*, **165**, 593–9.

Eggler DH, Mysen BO, Hoering TC (1979) The solubility of carbon monoxide in silicate melts at high pressures and its effect on silicate phase relations. *Earth and Planetary Science Letters*, **43**, 321–30.

Eugster HP, Skippen GB (1967) Igneous and metamorphic reactions involving gas equilibria. *Researches in Geochemistry*, **2**, 492–520.

Facq S, Daniel I, Montagnac G, Cardon H, Sverjensky DA (2014) In situ Raman study and thermodynamic model of aqueous carbonate speciation in equilibrium with aragonite under subduction zone conditions. *Geochimica et Cosmochimica Acta*, **132**, 375–90.

Foley SF, Yaxley GM, Rosenthal A, Buhre S, Kiseeva ES, Rapp RP, Jacob DE (2009) The composition of near-solidus melts of peridotite in the presence of CO_2 and H_2O between 40 and 60 kbar. *Lithos*, **1125**, 274–83.

Frezzotti ML, Di Vincenzo G, Ghezzo C, Burke EAJ (1994) Evidence of magmatic CO_2-rich fluids in peraluminous graphite-bearing leucogranites from Deep Freeze Range (northern Victoria Land, Antarctica). *Contributions to Mineralogy and Petrology*, **117**, 111–23.

Frezzotti ML, Selverstone J, Sharp ZD, Compagnoni R (2011) Carbonate dissolution during subduction revealed by diamond-bearing rocks from the Alps. *Nature Geoscience*, **4**, 703–6.

Galvez M, Alexander J, Connolly D (2015) The solubility of rocks in metamorphic fluids : a model for rock-dominated conditions to upper mantle pressure and temperature. *Earth and Planetary Science Letters*, **430**, 486–98.

Goncharov AG, Ionov DA, Doucet LS, Pokhilenko LN (2012) Thermal state, oxygen fugacity and C–O–H fluid speciation in cratonic lithospheric mantle: new data on peridotite xenoliths from the Udachnaya kimberlite, Siberia. *Earth and Planetary Science Letters*, **357**, 99–110.

Grassi D, Schmidt MW (2011) The melting of carbonated pelites from 70 to 700 km depth. *Journal of Petrology*, **4**, 765–89.

Holloway JR, Jakobsson S (1986) Volatile solubilities in magmas: transport of volatiles from mantles to planet surfaces. *Journal of Geophysical Research: Solid Earth (1978–2012)*, **91**, 505–8.

Holloway JR, Reese RL (1974) The generation of N_2–CO_2–H_2O fluids for use in hydrothermal experimentation I: experimental method and equilibrium calculations in the C–O–H–N system. *American Mineralogist*, **59**, 587–97.

Holloway JR, Burnham CW, Millhollen GL (1968) Generation of H_2O–CO_2 Mixtures for use in hydrothermal Experimentation. *Journal of Geophysical Research*, **73**, 6598–600.

Huizenga JM (2001) Thermodynamic modelling of C–O–H fluids. *Lithos*, **55**, 101–14.

Huizenga JM (2011) Thermodynamic modelling of a cooling C–O–H fluid–graphite system: implications for hydrothermal graphite precipitation. *Mineralium Deposita*, **46**, 23–33.

Jakobsson S, Holloway JR (1986) Crystal—Liquid experiments in the presence of a COH fluid buffered by graphite + iron + wustite: experimental method and near-liquidus relations in basanite. *Journal of Volcanology and Geothermal Research*, **29**, 265–91.

Jakobsson S, Holloway JR (2008) Mantle melting in equilibrium with an Iron–Wustite–Graphite buffered COH-fluid. *Contributions to Mineralogy and Petrology*, **155**, 247–56.

Jakobsson S, Oskarsson N (1990) Experimental determination of fluid composition in the system COH at high P and T and low fO_2. *Geochimica et Cosmochimica Acta*, **54**, 355–62.

Jakobsson S, Oskarsson N (1994) The system CO in equilibrium with graphite at high pressure and temperature: an experimental study. *Geochimica et Cosmochimica Acta*, **58**, 9–17.

Kerrick DM, Jacobs GK (1981) A modified Redlich-Kwong equation for H_2O, CO_2 and H_2O-CO_2 mixtures at elevated temperatures and pressures. *American Journal of Science*, **281**, 735–67.

Kesson SE, Holloway JR (1974) Generation of N_2–CO_2–H_2O fluids for use in hydrothermal experimentation. II. Melting of albite in a multispecies fluid. *American Mineralogist*, **59**, 598–603.

Kushiro I, Hirose K (1992) Experimental determination of composition of melt formed by equilibrium partial melting of peridotite at high pressures using aggregates of diamond grains. *Proceedings of the Japan Academy, Series B*, **68**, 63–8.

Lamadrid HM, Lamb WM, Santosh M, Bodnar RJ (2014) Raman spectroscopic characterization of H_2O in CO_2-rich fluid inclusions in granulite facies metamorphic rocks. *Gondwana Research*, **26**, 301–10.

Litvinosky BA, Steele IANM, Wickam SM (2000) Silicic magma formation in overthickened crust: melting of charnockite and leucogranite at 15, 20 and 25 kbar. *Journal of Petrology*, **41**, 717–37.

Luth RW (1989) Natural versus experimental control of oxidation state: effects on the composition and speciation of COH fluids. *American Mineralogist*, **74**, 50–7.

Malaspina N, Tumiati S (2012) The role of C-O-H and oxygen fugacity in subduction-zone garnet peridotites. *European Journal of Mineralogy*, **24**, 607–18.

Malaspina N, Scambelluri M, Poli S, Van Roermund HLM, Langenhorst F (2010) The oxidation state of mantle wedge majoritic garnet websterites metasomatised by C bearing subduction fluids. *Earth and Planetary Science Letters*, **298**, 417–26.

Manning CE, Boettcher SL (1994) Rapid-quench hydrothermal experiments at mantle pressures and temperatures. *American Mineralogist*, **79**, 1153–8.

Matveev S, Ballhaus C, Fricke K, Truckenbrodt J, Ziegenbein D (1997) CHO volatiles under upper mantle conditions. I. Experimental results. *Geochimica et Cosmochimica Acta*, **61**, 3081–8.

McCubbin FM, Sverjensky DA, Steele A, Mysen BO (2014) In-situ characterization of oxalic acid breakdown at elevated P and T: implications for organic C-O-H fluid sources in petrologic experiments. *American Mineralogist*, **99**, 2258–71.

Melekhova E, Schmidt MW, Ulmer P, Pettke T (2007) The composition of liquids coexisting with dense hydrous magnesium silicates at 11–13.5 GPa and the endpoints of the solidi in the MgO–SiO_2–H_2O system. *Geochimica et Cosmochimica Acta*, **71**, 3348–60.

Morgan GB, Chou I, Pasteris JD (1992) Speciation in experimental COH fluids produced by the thermal dissociation of oxalic acid dihydrate. *Geochimica et Cosmochimica Acta*, **56**, 281–94.

Mysen BO, Yamashita S (2010) Speciation of reduced C-O-H volatiles in coexisting fluids and silicate melts determined in-situ to 1.4 GPa and 800°C. *Geochimica et Cosmochimica Acta*, **74**, 4577–88.

Newton RC, Manning CE (2000) Quartz solubility in H2O-NaCl and H2O-CO2 solutions at deep crust-upper mantle pressures and temperatures: 2–15 kbar and 500–900°C. *Geochimica et Cosmochimica Acta*, **64**, 2993–3005.

Newton RC, Manning CE (2009) Hydration state and activity of aqueous silica in H_2O-CO_2 fluids at high pressure and temperature. *American Mineralogist*, **94**, 1287–90.

Olafsson M, Eggler DH (1983) Phase relations of amphibole, amphibole-carbonate, and phlogopite-carbonate peridotite: petrologic constraints on the asthenosphere. *Earth and Planetary Science Letters*, **64**, 305–15.

Pan D, Spanu L, Harrison B, Sverjensky DA, Galli G (2013) Dielectric properties of water under extreme conditions and transport of carbonates in the deep Earth. *Proceedings of the National Academy of Sciences*, **110**, 6646–50.

Pasteris JD (1987) Fluid inclusions in mantle xenoliths. In: *Mantle Xenoliths* (ed. Nixon PH), pp. 691–707. Wiley, Chichester.

Pernert JC (1952) Oxalic acid. *Encyclopaedia of Chemical Technology*, **9**, 661–74.

Poli S, Franzolin E, Fumagalli P, Crottini A (2009) The transport of carbon and hydrogen in subducted oceanic crust: an experimental study to 5 GPa. *Earth and Planetary Science Letters*, **278**, 350–60.

Pownceby MI, O'Neill HSC (1994) Thermodynamic data from redox reactions at high temperatures. IV. Calibration of the Re-ReO_2 oxygen buffer from EMF and NiO + Ni-Pd redox sensor measurements. *Contributions to Mineralogy and Petrology*, **118**, 130–7.

Roedder E (1965) Liquid CO_2 inclusions in olivine-bearing nodules and phenocrysts from basalts. *American Mineralogist*, **50**, 1746.

Rosenbaum JM, Slagel MM (1995) COH speciation in piston-cylinder experiments. *American Mineralogist*, **80**, 109–14.

Sanchez-Valle C, Martinez I, Daniel I, Philippot P, Bohic S, Simionovici A (2003) Dissolution of strontianite at high PT conditions: an in-situ synchrotron X-ray fluorescence study. *American Mineralogist*, **88**, 978–85.

Schmidt C (2014) Raman spectroscopic determination of carbon speciation and quartz solubility in H2O + Na2CO3 and H2O + NaHCO3 fluids to 600°C and 1.53 GPa. *Geochimica et Cosmochimica Acta*, **145**, 281–96.

Schmidt MW, Ulmer P (2004) A rocking multianvil: elimination of chemical segregation in fluid-saturated high-pressure experiments. *Geochimica et Cosmochimica Acta*, **68**, 1889–99.

Shmulovich KI, Yardley BWD, Graham CM (2006) Solubility of quartz in crustal fluids: experiments and general equations for salt solutions and H2O–CO2 mixtures at 400–800°C and 0.1–0.9 GPa. *Geofluids*, **6**, 154–67.

Stagno V, Frost DJ, McCammon CA, Mohseni H, Fei Y (2015) The oxygen fugacity at which graphite or diamond forms from carbonate-bearing melts in eclogitic rocks. *Contributions to Mineralogy and Petrology*, **169**, 1–18.

Stalder R, Ulmer P (2001) Phase relations of a serpentine composition between 5 and 14 GPa: significance of clinohumite and phase E as water carriers into the transition zone. *Contributions to Mineralogy and Petrology*, **140**, 670–9.

Sverjensky DA, Harrison B, Azzolini D (2014) Water in the deep Earth: the dielectric constant and the solubilities of quartz and corundum to 60 kb and 1200°C. *Geochimica et Cosmochimica Acta*, **129**, 125–45.

Taylor WR, Foley SF (1989) Improved oxygen-buffering techniques for C-O-H fluid saturated experiments at high pressure. *Journal of Geophysical Research: Solid Earth (1978–2012)*, **94**, 4146–58.

Taylor WR, Green DH (1988) Measurement of reduced peridotite–COH solidus and implications for redox melting of the mantle. *Nature*, **332**, 349–52.

Thibault Y, Edgar AD, Lloyd FE (1992) Experimental investigation of melts from a carbonated phlogopite lherzolite: implications for metasomatism in the continental lithospheric mantle. *American Mineralogist*, **77**, 784–94.

Thomsen TB, Schmidt MW (2008) Melting of carbonated pelites at 2.5–5.0 GPa, silicate carbonatite liquid immiscibility, and potassium–carbon metasomatism of the mantle. *Earth and Planetary Science Letters*, **267**, 17–31.

Truckenbrodt J, Johannes W (1999) H_2O loss during piston-cylinder experiments. *American Mineralogist*, **84**, 1333–5.

Truckenbrodt J, Ziegenbein D, Johannes W (1997) Redox conditions in piston cylinder apparatus: the different behavior of boron nitride and unfired pyrophyllite assemblies. *American Mineralogist*, **82**, 337–44.

Tumiati S, Fumagalli P, Tiraboschi C, Poli S (2013) An Experimental Study on COH-bearing Peridotite up to 3.2 GPa and implications for crust–mantle recycling. *Journal of Petrology*, **54**, 453–79.

Wallace ME, Green DH (1988) An experimental determination of primary carbonatite magma composition. *Nature*, **335**, 343–6.

Walther JV, Orville PM (1983) The extraction-quench technique for determination of the thermodynamic properties of solute complexes: application to quartz solubility in fluid mixtures. *American Mineralogist*, **68**, 731–41.

Wyllie PJ (1978) Mantle fluid compositions buffered in peridotite by carbonates, amphibole, and phlogopite. *The Journal of Geology*, **86**, 687–713.

Zhang C, Duan Z (2009) A model for C-O–H fluid in the Earth's mantle. *Geochimica et Cosmochimica Acta*, **73**, 2089–102.

Zhang C, Duan Z (2010) GFluid: an Excel spreadsheet for investigating C–O–H fluid composition under high temperatures and pressures. *Computers & Geosciences*, **36**, 569–72.

SUPPORTING INFORMATION

Additional Supporting Information may be found online in the supporting information tab for this article:

Figure S1. COH ternary diagram. Green solid line: graphite saturation surface (Connolly 1995).

Table S1. Calibration matrix. Contribution of the chemical species of interest for every m/z channel monitored from the calibration procedure performed with three different gas mixtures, water and air (see main text).

Appendix S1. Thermodynamic modeling of COH fluids.